Electromagnetic Non-Destructive Evaluation (XXI)
D. Lesselier and C. Reboud (Eds.)

doi:10.3233/978-1-61499-836-5-96

B-Spline Sparse Grids for Eddy-Current Testing Inverse Problems

Sándor BILICZ [1] and József PÁVÓ
Budapest University of Technology and Economics, Hungary

Abstract. A sparse grid surrogate model using hierarchical B-spline basis functions is used to approximate the objective function in an optimization-based inversion algorithm. The B-spline basis provides a smooth interpolant of the objective function and the gradient of the interpolant is readily available in closed-form. The latter is used in a gradient-based minimum search algorithm that results in the approximate solution of the inverse problem. The method is computationally more efficient than using gradient-free direct search methods, as illustrated by an example drawn from eddy-current nondestructive testing.

Keywords. inverse problem, sparse grid, B-spline, gradient-based optimization

1. Introduction

Surrogate models can facilitate the solution of inverse problems related to electromagnetic nondestructive evaluation. The benefit from a surrogate model is the cheap approximation of the usually heavy electromagnetic simulation. In this way, the model-based inversion—that relies on several subsequent evaluations of the forward model—can be significantly sped up.

Most surrogate modeling approaches consist in the interpolation of the input-output function based on its pre-calculated samples (training data or database). Various sampling and interpolation techniques have been applied in the context of electromagnetic nondestructive testing (NdT). The adaptive mesh-databases combined with linear [1], [2] or radial basis function interpolation [3] have been shown to apply well as surrogate models. Later, to cope with the curse-of-dimensionality (i.e., the exponential increase of storage and computational needs of the surrogate model with increasing number of input parameters), sparse grid surrogate models have been introduced. Traditionally, piecewise linear basis functions were used for the interpolation on sparse grids [4]. The efficiency of the method in the context of computational electromagnetics has been demonstrated, e.g., in [5]. In eddy-current nondestructive testing (EC-NdT), the inverse problem has also been targeted with sparse grids. A Monte Carlo sampling was built on the surrogate in [6], to jointly perform model selection and optimisation-based inversion. The idea of sparse grids in EC-NdT inversion is flashed also in other contributions, e.g., [7].

A bottleneck of piecewise linear interpolation (which is common with sparse grids) is the lack of continuous derivatives of the interpolant with respect to the input param-

[1]Corresponding Author: Sándor Bilicz; E-mail: bilicz@evt.bme.hu

eters. This hinders the use of gradient-based algorithms of inversion through the optimization of a misfit function. This is the main motivation for using hierarchical B-splines as basis functions, e.g., in [8]. This technique yields a smooth interpolant of which the gradient is continuous and can be analytically expressed.

In the present work, the sparse grid surrogate model with hierarchical B-spline basis functions is outlined (Sec. 2) and its use for optimization-based inversion is presented (Sec. 3). Finally, a numerical example drawn from EC-NdT is discussed (Sec. 4).

2. Sparse grid interpolation with hierarchical B-spline basis functions

Let us consider a flaw model (e.g., a crack or void) with N parameters, each having lower and upper bounds. The region of interest in terms of parameters $\mathbf{x} = [x_1, \ldots, x_N]$ is thus an N-dimensional space. Let us assume that the allowed domain of the parameters—say, the *input space*—is the N-dimensional unit-hypercube $[0,1]^N$ (this is possible in most practical cases by some appropriate transformation of the parameters). The output signal (e.g., a surface scan of impedance variation of a probe coil) corresponding to the parameter vector $\mathbf{x}$ is denoted by $\mathbf{y} = \mathbf{f}(\mathbf{x})$. The vector-vector function $\mathbf{f}$ represents the NdT forward problem as an input-output function, and $\mathbf{f}$ is usually evaluated by means of numerical simulation, involving a brute-force method such as the finite element or the moment method. To reduce the computational burden associated with the evaluation of $\mathbf{f}$, one seeks for an approximation $\hat{\mathbf{f}} \approx \mathbf{f}$, i.e., the surrogate model of the original problem.

To this end, sparse grid interpolation is proposed, which is briefly summarized as:

1. definition of a hierarchical set of basis functions in 1-dimension (1-D);
2. generation of a set of hierarchical N-D basis functions as tensor product of the 1-D bases;
3. truncation of the set of N-D basis functions such that the resulting set is "sparse" in a certain sense.

Let us denote the set of 1-D basis functions at level ℓ by

$$\Psi_\ell(x) = \left\{ \psi_i^{(\ell)}(x) \;\middle|\; i = 1,2,\ldots,m_\ell^{(1)} \right\} \tag{1}$$

where $\ell = 0,1,2,\ldots,d$, with d being the depth of the hierarchical interpolation. The sparse tensor product [4] of N number of such 1-D bases at its level ℓ is given by

$$\Phi_\ell(\mathbf{x}) = \left\{ \Psi_{\ell_1}(x_1) \otimes \Psi_{\ell_2}(x_2) \otimes \cdots \otimes \Psi_{\ell_N}(x_N) \;\middle|\; \sum_{i=1}^{N} \ell_i = \ell \right\}. \tag{2}$$

A linear truncation is used herein, i.e., all N-D basis functions involved in a depth=d interpolation satisfy the linear constraint for the level indices $\sum_{i=1}^{N} \ell_i \le d$. With this sparse hierarchical basis, the interpolant $\hat{\mathbf{f}}$ has the form of

$$\hat{\mathbf{f}}(\mathbf{x}) = \sum_{\ell=0}^{d} \sum_{i=1}^{m_\ell^{(N)}} \mathbf{c}_i^{(\ell)} \boldsymbol{\phi}_i^{(\ell)}(\mathbf{x}), \tag{3}$$

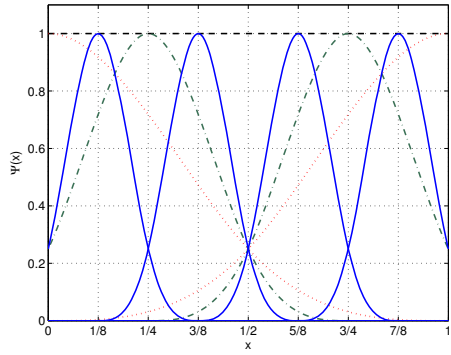

Figure 1. Hierarchical B-splines ($\psi_i^{(\ell)}(x)$) of order 3. Level 0 (- - -), level 1 ($\cdots$), level 2 (- · -) and level 3 (—) basis functions.

where $\mathbf{c}_i^{(\ell)}$ and $\phi_i^{(\ell)}(\mathbf{x})$ are the i-th vectorial coefficient and the related basis function at level ℓ, the latter is an element of $\Phi_\ell(\mathbf{x})$ in (2), and $m_\ell^{(N)}$ is the number of basis functions at level ℓ in an N-D sparse grid, respectively.

Linear ("hat") basis functions $\psi_i^{(\ell)}(x)$ are commonly used with sparse grids. In the present work, *hierarchical* B-spline basis functions are applied, and similarly to [8], 3rd order B-splines have been chosen. This choice ensures the continuity of the 2nd order derivatives of interpolant (3). The 3rd order *cardinal* B-spline is defined in the interval $0 \le x \le 4$ and it is expressed as

$$b^{(3)}(x) = \begin{cases} {}^1\!/\!_4 x^3, & 0 \le x < 1; \\ -{}^3\!/\!_4 x^3 + 3x^2 - 3x + 1, & 1 \le x < 2; \\ {}^3\!/\!_4 x^3 - 6x^2 + 15x - 11, & 2 \le x < 3; \\ -{}^1\!/\!_4 x^3 + 3x^2 - 12x + 16, & 3 \le x \le 4. \end{cases} \tag{4}$$

In our implementation, the level 0 basis function is chosen as constant ($\psi_1^{(1)}(x) = 1$) and all other hierarchical basis functions ($\ell \ge 1$) are derived from a cardinal B-spline (4) via an affine transformation of the input variable, as illustrated in Fig. 1.

To determine the coefficients $\mathbf{c}_i^{(\ell)}$ in (3), the equality $\hat{\mathbf{f}}(\mathbf{x}_k) = \mathbf{f}(\mathbf{x}_k)$ is enforced at n number of control points ($\mathbf{x}_k, k = 1, 2, \ldots, n$). These points are chosen as the center points of the corresponding basis functions (i.e., where $\phi_i^{(\ell)}(\mathbf{x}) = 1$ hold, for all $\ell \ge 1$, and by definition, it is ${}^1\!/\!_2[1, 1, \ldots, 1]$ for $\phi_1^{(0)}(\mathbf{x})$). The number of control points is thus equal to the cardinality of the sparse basis (2), and the location of the set of these control points (nodes) forms the so-called *sparse grid*. In 2-D, the distribution of the sparse grid nodes is illustrated in Fig. 2, along with the contour lines of the sparse grid interpolant of the well-known Branin test function [9].

The sparse grid interpolation can cope with the curse-of-dimensionality in the following sense. The number of grid nodes n in a sparse grid with depth d in dimension N is in the order $\mathcal{O}\{K(\log K)^{N-1}\}$, where $K = 2^d + 1$ being the number of hierarchical basis functions per dimension. However, the increase of n is much faster when a classical full grid is used, herein $\mathcal{O}\{K^N\}$ applies [4]. The numerical example presented in Sec. 4 involves $N = 4$ dimensions, for which the node numbers of sparse and full grids

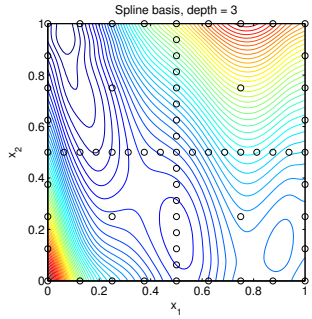

Figure 2. Contour lines of the interpolant of the Branin test function by means of a depth=3 sparse grid with hierarchical B-spline basis functions, along with the grid nodes.

Table 1. Node numbers of sparse and full grids in $N = 4$ dimension, in function of the depth d.

d	0	1	2	3	4	5	6
n (sparse)	1	9	41	137	401	1105	2929
n (full)	1	81	625	6561	83521	1185921	17850625

are compared in Table 1 as an illustration of the gain benefited from sparse grids. In spite of the large reduction of node numbers, the interpolation accuracy of sparse grids is only slightly deteriorated compared to full grids, as detailed in [4].

3. Inversion using the sparse grid surrogate model

Once the sparse grid surrogate model (3) is available, and hierarchical B-splines are used as basis functions therein, one can solve the inverse problem by means of optimizing a misfit function, as it follows. Let us assume that the output $\mathbf{y}$ of the numerical simulation $\mathbf{f}(\mathbf{x})$ (as already mentioned in Sec. 2) is a real row vector of M elements: $\mathbf{y} = [y_1, y_2, \ldots, y_M]$. In the case of complex output (e.g., complex impedance variation in EC-NdT), one can always introduce the real output vector as $\mathbf{y} \coloneqq [\mathrm{Re}\{\mathbf{y}\}, \mathrm{Im}\{\mathbf{y}\}]$. The measured data vector is denoted by $\tilde{\mathbf{y}}$. Let us define the quadratic misfit function as the squared norm of the discrepancy between simulated and measured data:

$$u(\mathbf{x}) = \|\tilde{\mathbf{y}} - \mathbf{y}\|^2 \equiv [\tilde{\mathbf{y}} - \mathbf{y}][\tilde{\mathbf{y}} - \mathbf{y}]^{\mathsf{T}} \tag{5}$$

The regularized inverse problem then consists in solving the constrained optimization problem

$$\mathbf{x}' = \underset{\mathbf{x}\in[0,1]^N}{\arg\min}\, u(\mathbf{x}) \tag{6}$$

that yields the solution $\mathbf{x}'$. In order to reduce the computational burden, one approximates $\mathbf{y} = \mathbf{f}(\mathbf{x})$ by $\hat{\mathbf{y}} = \hat{\mathbf{f}}(\mathbf{x})$, and the approximate misfit function $\hat{u}(\mathbf{x}) = \|\tilde{\mathbf{y}} - \hat{\mathbf{y}}\|^2$ is to be minimized according to (6). Since $\hat{\mathbf{f}}(\mathbf{x})$ is based on a sparse grid interpolation with hierarchical B-spline basis functions, its gradient

$$\nabla\hat{\mathbf{f}}(\mathbf{x}) = \begin{bmatrix} \partial\hat{y}_1/\partial x_1 & \partial\hat{y}_2/\partial x_1 & \cdots & \partial\hat{y}_M/\partial x_1 \\ \vdots & & \ddots & \vdots \\ \partial\hat{y}_1/\partial x_N & \partial\hat{y}_2/\partial x_N & \cdots & \partial\hat{y}_M/\partial x_N \end{bmatrix} \tag{7}$$

can be easily expressed in closed form based on (3). Therefore, one can also write the gradient of the quadratic approximate misfit function in closed form (see, e.g., [10]) as

$$\nabla\hat{u}(\mathbf{x}) = 2[\tilde{\mathbf{y}} - \hat{\mathbf{f}}(\mathbf{x})][\nabla\hat{\mathbf{f}}(\mathbf{x})]^{\mathsf{T}}. \tag{8}$$

This gradient (8) can be used in the gradient-based solution of the optimization problem (6). In order that one can choose among the large variety of classical unconstrained optimization algorithms, the constrained problem (6) has to be re-formulated by using some nonlinear transformation of the optimization variable $\mathbf{x}$. Herein a new variable $\xi = [\xi_1, \xi_2, \ldots, \xi_N]$ is introduced such that

$$x_i = (\arctan\xi_i)/\pi + 1/2, \quad x_i \in [0,1], \quad \xi_i \in (-\infty,\infty), \quad i = 1,2,\ldots,N, \tag{9}$$

and the optimization is performed with respect to ξ in an unconstrained domain:

$$\xi' = \underset{\xi\in\mathbb{R}^N}{\arg\min}\, u(\mathbf{x}(\xi)). \tag{10}$$

The gradient-based local optimization strategies unfortunately suffer from the possibility of stalling in a local minimum and thus miss the global minimum. This risk is reduced when one runs the algorithm with different initial guesses. However, this was not the case in the numerical example which is presented in the next section.

4. Numerical example

4.1. Configuration

Let us consider the eddy-current testing arrangement shown in Fig. 3. A homogeneous, non-ferromagnetic plate is considered as specimen. The conductivity is $\sigma = 10^6\,\mathrm{S/m}$ and the thickness is $t = 1.55\,\mathrm{mm}$. The other dimensions of the plate are assumed to be infinite. The coil is an air-cored probe (inner and outer diameters: 2 mm and 3.25 mm; height: 2 mm; no. of turns: 328; lift-off h: 0.303 mm), driven with a time-harmonic current with frequency of 300 kHz. The variation of the coil impedance is observed at regularly spaced coil positions:

$$x_c = \{-15 : 1 : 15\}\,\mathrm{mm} \quad \text{and} \quad y_c = \{-5 : 1 : 5\}\,\mathrm{mm}, \tag{11}$$

that is, $31 \times 11 = 341$ complex impedance variations are available in the surface scan.

A rectangular-shaped defect (with zero conductivity) is present within the plate, with sides parallel to the x, y and z axes; the defect is centered on the origin of the xy plane. The bounds given in Table 2 apply for the 4 geometrical parameters of the defect. The input domain is non-rectangular but narrowed by a linear inequality constrain for d and l. This

Table 2. Parameter ranges in the single narrow crack example.

parameter		range
length	a	$[4, 22]$mm
width	b	$[0.001, 0.3]$mm
depth	d	$[10, 100]$% (of plate thickness)
ligament	l	$[0, t-d]$

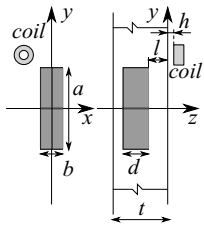

Figure 3. Sketch of the configuration.

is taken into account when transforming the input domain to the $[0,1]^N$ hypercube, on which the sparse grid and inversion algorithms are performed, as already seen in Sec. 2.

The electromagnetic simulation is based on an integral equation formulation, implemented in the CIVA software [11].

4.2. Test of the forward interpolation

The interpolation error is defined as $\varepsilon(\mathbf{x}) = \|\hat{f}(\mathbf{x}) - \mathbf{f}(\mathbf{x})\|$ at each point $\mathbf{x}$. The overall interpolation performance is characterized by the maximal and root mean-squared (rms) interpolation error, both are approximated based on a finite number of test samples $\mathbf{x}_j$ ($j = 1,2,\ldots,J$):

$$\varepsilon_{\max} = \max_j \varepsilon(\mathbf{x}_j), \qquad \varepsilon_{\mathrm{rms}} = \sqrt{\frac{1}{J}\sum_j \varepsilon(\mathbf{x}_j)^2} \tag{12}$$

In this numerical test, 4000 random test samples are used. In order to facilitate the interpretation of the error, the normalized (dimensionless) interpolation error is presented, with a normalizing factor that is chosen as $\max_j \|\mathbf{f}(\mathbf{x}_j)\|$. The change of the normalized error with respect to the depth of the sparse grid interpolation is shown in Fig. 4. For reference, linear basis functions [5] have also been used. In terms of interpolation accuracy, the linear basis slightly outperforms the B-splines. Yet, the B-splines are better in optimization-based inversion schemes, as shown in the next section.

4.3. Test of the inversion algorithm

As summarized in Table 3, the output signal associated with two randomly chosen defects (denoted as "true") has been calculated. The inversion procedure detailed in Sec. 3 resulted in the reconstructed parameters denoted as "grad". For comparison, a similar optimization-based inversion has been performed using the sparse grid with linear basis functions (the same as presented in the previous section). Due to the lack of continuous

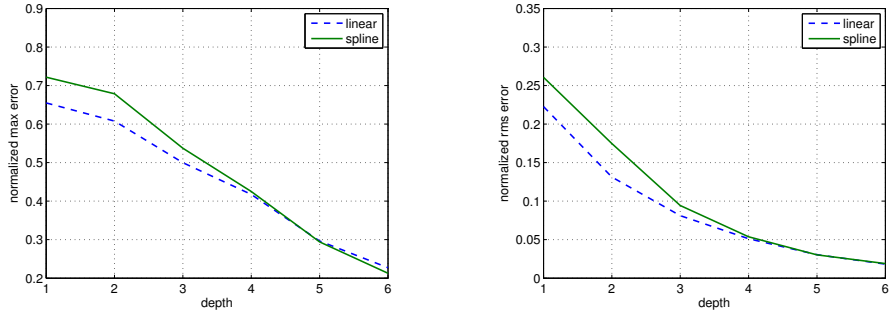

(a) maximal error (b) rms error

Figure 4. Normalized interpolation error in the numerical example.

Table 3. Results of the inversion in the 1st (*left*) and 2nd (*right*) test cases. The "true" parameters correspond to the defect to be reconstructed, and the gradient-based ("grad") and simplex optimisation-based ("direct") inversion methods yielded the parameters as given in the tables. Depth=6 sparse grid is used in all cases.

	a	*b*	*d*	*l*
true	**16.04**	**0.290**	**0.258**	**0.413**
grad	16.30	0.012	0.474	0.324
direct	20.42	0.118	0.348	0.389

	a	*b*	*d*	*l*
true	**15.10**	**0.157**	**0.525**	**0.942**
grad	14.96	0.188	0.507	0.957
direct	16.20	0.137	0.478	0.850

gradient of the interpolant, a simplex optimization (referred to as "direct") method has been applied with the linear basis. According to Table 3, both approaches found reliable solutions, except for parameter b, which is the width of the defect and it is well-known to have only a weak influence on the impedance change. This measurement setup thus has limited capacity in reconstructing b.

The main advantage of the B-spline based scheme becomes clear when looking at the evolution of the iterative optimization routines in Fig. 5. In both examples, the gradient method converged much faster to a better local minimum than the simplex method.

Implementation has been made in Matlab, with the functions `fminunc` (a quasi-Newton method) and `fminsearch` (a simplex method for direct search).

5. Conclusion

The use of B-spline basis functions for interpolation on sparse grids has been found to be an efficient tool when performing optimization-based inversion using the sparse grid surrogate model. The gradient of the approximate misfit function is continuous, giving rise to gradient methods. Spare grids *per se* have previously proven a good performance in NdT inversion; and the present contribution is an extension of this solid framework.

Future work will include the expression the Hessian of the misfit function to use second order optimization methods. Furthermore, one will study the case when the gradient of the forward model $\mathbf{f}$ is available at hand (e.g., via the adjoint problem), and it can be used to fit the surrogate model not only to $\mathbf{f}$ but to $\nabla\mathbf{f}$ as well. Considerations on the adaptive generation of the sparse grid in combination with B-spline basis functions will also be taken.

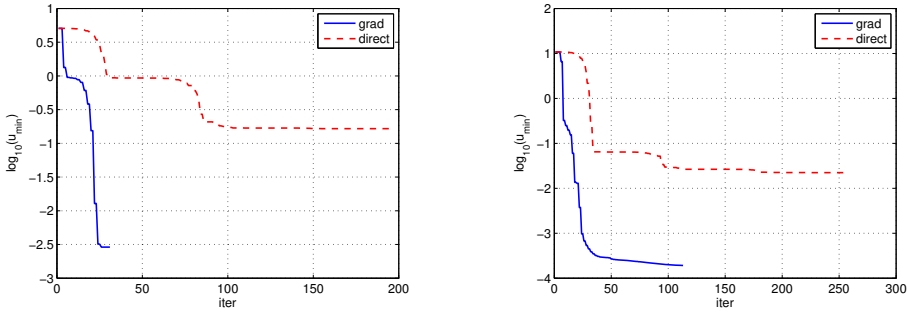

(a) 1st test case (b) 2nd test case

Figure 5. Performance of the inversion with gradient-based ("grad") and simplex optimisation-based ("direct") inversion methods: minimum misfit function found with respect to iteration number.

Acknowledgment

The work was created in commission of the National University of Public Service under the priority project KÖFOP-2.1.2-VEKOP-15-2016-00001 titled "Public Service Development Establishing Good Governance" in the Bay Zoltán Ludovika Workshop. Further support was provided by the Hungarian Scientific Research Fund under grant K-111987 and by the János Bolyai Research Scholarship of the Hungarian Academy of Sciences.

References

[1] G. Franceschini, M. Lambert, and D. Lesselier, "Adaptive database for eddy-current testing of metal tube," in *Proceedings of the 8th International Symposium on Electric and Magnetic Fields (EMF 2009)*, Mondovi, Italie, May 2009, (on CDROM).

[2] S. Gyimóthy, "Optimal sampling for fast eddy current testing inversion by utilising sensitivity data," *IET Science, Measurement & Technology*, vol. 9, no. 3, pp. 235 – 240, 2015.

[3] R. Douvenot, M. Lambert, and D. Lesselier, "Adaptive metamodels for crack characterization in eddy-current testing," *IEEE Transactions on Magnetics*, vol. 47, no. 4, pp. 746–755, 2011.

[4] H.-J. Bungartz and M. Griebel, "Sparse grids," *Acta Numerica*, vol. 13, pp. 147–269, 2004.

[5] S. Bilicz, "Sparse grid surrogate models for electromagnetic problems with many parameters," *IEEE Transactions on Magnetics*, vol. 52, no. 3, pp. 1–4, 2016.

[6] C. Cai, S. Bilicz, T. Rodet, M. Lambert, and D. Lesselier, "Metamodel-based nested sampling for model selection in eddy-current testing," *IEEE Transactions on Magnetics*, vol. 53, no. 4, pp. 1–8, 2017.

[7] L. Zhou, H. A. Sabbagh, E. H. Sabbagh, R. K. Murphy, W. Bernacchi, J. C. Aldrin, D. Forsyth, and E. Lindgren, "Eddy-current NDE inverse problem with sparse grid algorithm," *AIP Conference Proceedings*, vol. 1706, no. 1, p. 090016, 2016.

[8] J. Valentin and D. Pflüger, *Sparse Grids and Applications - Stuttgart 2014*. Springer International Publishing Switzerland, 2016, ch. Hierarchical Gradient-Based Optimization with B-Splines on Sparse Grids, pp. 315–336.

[9] A. Forrester, A. Sobester, and A. Keane, *Engineering design via surrogate modelling: a practical guide*. Wiley, 2008.

[10] A. Tarantola, *Inverse Problem Theory and Model Parameter Estimation*. SIAM, 2005.

[11] CIVA: A state-of-art simulation software in ndt. [Online]. Available: http://www.extende.com